Results in Physics 12 (2019) 349–356

Contents lists available at ScienceDirect

Results in Physics

journal homepage: www.elsevier.com/locate/rinp

Performance optimization design and analysis of bearingless induction motor with different magnetic slot wedges

Ke Li[a], Guoyu Cheng[a], Xiaodong Sun[b,*], Zebin Yang[a], Yeman Fan[c]

[a] Automotive Engineering Research Institute, Jiangsu University, Zhenjiang 212013, Jiangsu, China
[b] School of Electrical and Information Engineering, Jiangsu University, Zhenjiang 212013, Jiangsu, China
[c] College of Mechanical and Electronic Engineering, Northwest A&F University, Yangling 712100, Shaanxi, China

ARTICLE INFO

Keywords:
Bearingless motor
Magnetic wedges
Induction motor
Finite element analysis

ABSTRACT

This paper investigates the application of using magnetic wedges in a semi-closed slot bearingless induction (BI) motor. In this strategy, the electrical loss of the motor can be reduced, improving the overall efficiency. At the same time, the temperature rise of the winding is reduced, and the vibration and noise levels are greatly depressed, which prolong the service life of the motor. First, the principle of BI motor operation is introduced. Second, the different magnetic permeability and geometric shape of the magnetic wedge are taken into consideration during the analysis the proposed BI motor. Then, the performance of BI motor with magnetic wedge is analyzed by finite element method. Finally, the results show that too high relative permeability materials can degrade the performance of the BI motor, thus, the use of suitable permeable magnetic wedge is reasonable. After adding the optimal magnetic wedge, the torque ripple, motor efficiency and the suspension force of the BI motor are optimized. The use of magnetic wedges has economic advantages and is of great significance for improving the performance of BI motors.

Introduction

High and ultra-high speed motors have developed rapidly in the industrial field because of their great power density advantages [1]. However, the traditional high-speed motor has the unavoidable shortcomings due to the existence of mechanical bearings, which limits its development and application in practice. Fortunately, the theory of magnetic bearings have been put forward and developed rapidly, so non-contact supporting motors are designed to overcome the shortcomings of mechanical bearings. Under the special circumstances of high speed, ultra-high speed, empty space, cleaning and abominable, motors without mechanical bearings can operate smoothly and correctly. In electronics, pharmaceuticals, flywheel energy storage, semiconductors, energy chemicals, flexible manufacturing, transmission systems, rail transit, life sciences and other high-tech industries, magnetic bearing motors have a broad application prospect [2–4].

It is well known that conventional magnetic bearing motors tend to be huge, requiring many single-phase inverters and a large number of wires [5]. According to the configuration similarities between magnetic bearings and conventional motors, various bearingless motors have been proposed and extensively studied, including bearingless induction (BI) motors, bearingless switched reluctance (BSR) motors, bearingless permanent magnet synchronous (BPMS) motors and so on [6–10]. The bearingless motor has a great deal of advantages over the magnetic bearing motor, such as greater critical velocity, a shorter shaft, and are more suitable for locations where ultra-high speed operation is required [11]. Among all kinds of bearingless motors, BI motors have obvious advantages, such as simple rotor structure, high precision and uniform air gap. In [12], an integration of magnetic bearings into the tubular linear actuator is proposed, resulting in a new, self-bearing (bearingless) tubular linear actuator. In [13], in order to improve the torque and suspension force performance of the bearingless synchronous reluctance motor, a multilayer reluctance rotor structure is proposed. The key is to optimize flux-barrier layer number, flux-barrier thickness, and magnetic guide thickness. In [14], a simple driving method is proposed. For an actively controlled 2-DOF bearingless motor, only one three-phase inverter is used. The radial suspension force is analytically calculated and verified by the finite element method. In [15], the BI motor that has separate windings was put forward and the fault tolerance of the motor was improved by independent control. It can be found that both the control strategy and the optimal design of the motor structure can improve the performance of the BI motor, and scholars at home and abroad are actively involved in motor optimization research.

The possibility of improving the efficiency of BI motors is becoming

* Corresponding author.
E-mail address: xdsun@ujs.edu.cn (X. Sun).

https://doi.org/10.1016/j.rinp.2018.11.078
Received 5 November 2018; Received in revised form 19 November 2018; Accepted 23 November 2018
Available online 01 December 2018

more and more limited [16]. Therefore, it is necessary to find new ways to reduce losses. Adding magnetic wedges to the stator slot is widely used in the manufacturers of medium-voltage BI motors [17–20]. The discontinuity in the gap caused by the existence of the slot produces harmonic components. The components create parasitic moments (and hence vibrations) in the motor, and there are harmonic components in the stator current, increasing copper and stray losses [21]. To improve space flux distribution and reduce its negative impact [22], semi-closed slots are used in low power motors with stochastic windings. In contrast, in large power motor, semi closed slot cannot be used because of the use of mounted windings. In this case, the use of open slot is an alternate, and then the existence of parasitic torque has become an important issue. In order to solve this problem, an effective solution is to add magnetic wedge into stator slot [23]. In this paper, the magnetic wedge is used to reduce the impact of semi closed slot, so as to improve the performance of the motor.

In [24], when the magnetic wedge was used to seal slot opening of the motor, the load current will decrease with the increase of efficiency and power factor. In addition, this article reveals that the use of excessively high permeability wedge material will reduce the efficiency of the motor. In [25], relative permeability and the magnetic wedge of different sizes of the motor were researched, and the effect on the motor starting performance was shown. Through simulation and experiment, it was found that the starting torque is increased and the starting current is reduced. After the magnetic wedge is used, the air gap coefficient of the generator is reduced, resulting in the decrease of excitation current and no-load current. In [26], the advantages of magnetic wedges that pay special attention to the economy were analyzed. The large motor performance to the highest level may lead to a great reduction in energy consumption. This article also describes a large motor research, as well as the use of magnetic wedge for energy-saving analysis.

This paper aims to contribute to the optimal design of BI motors. This proposal is particularly focused on improving efficiency. The paper is organized as follows. Section ‘BI motor operation principle’ introduces the BI motor operation principle. Section ‘Finite element analysis’ shows the effect of magnetic wedge on the performance of BI motors by the finite element analysis method. The significance of improving the BI motor performance is discussed in Section ‘Discussion’, followed by the conclusions in Section ‘Conclusion’.

BI motor operation principle

In order to achieve stable suspension of BI motor rotor, two sets of windings of different pole pairs are embedded in the stator slots. A set of winding pole-pair numbers is P_t and the magnetic field current frequency is ω_t. Another set of winding pole-pair numbers is P_s and the magnetic field current frequency is $\omega_s\omega_s$. When two sets of windings meet $P_tP_t = P_s \pm 1$ and $\omega_t = \omega_s$ [27,28], the motor can produce a controlled suspension force. Among them, the winding with a pole pair of P_t produces a rotating magnetic field and electromagnetic torque, it is called torque winding. Similarly, the winding with a pole pair of P_s produces the stable radial suspension force to realize the suspension of the rotor, which is called the suspension winding. Adding the suspension control winding breaks the balance of the rotating magnetic field generated by the torque control winding [29]. Then the magnetic field of the air gap area of the motor is strengthened, and the magnetic field in its spatially symmetric region is reduced, so that the resulting Maxwell force will be directed to the side where the magnetic field is enhanced [30].

Fig. 1 shows the principle of suspension force generation. ψ_1 and ψ_2 are flux linkages generated by the torque winding and the suspension winding, respectively. Assume that the effective resistance numbers of each phase of the torque and suspension winding are N_1 and N_2, respectively [31,32]. Currents introduced into the windings are I_1 and I_2, resulting in flux linkage $\psi_1\psi_1$ and ψ_2, respectively. The x and y represent

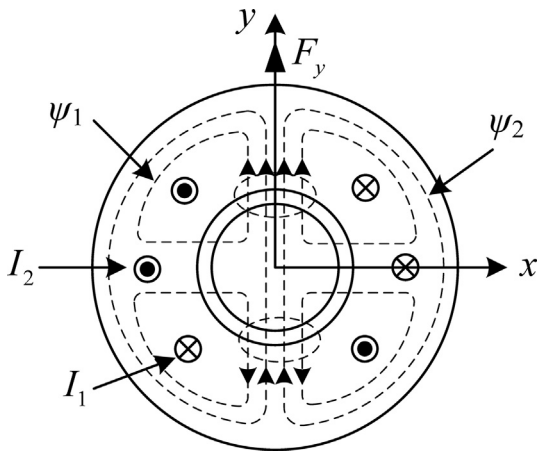

Fig. 1. BI motor suspension force generation principle.

the vertical rotor position control coordinate axis, respectively. The interaction of the magnetic fields generated by the two sets of windings can simultaneously generate radial suspension forces and electromagnetic torque. When the two windings pass through the current direction shown in Fig. 1, the air gap flux density is enhanced at the same direction in the upper air gap ψ_1 and ψ_2. However, the air gap flux density is attenuated in the opposite direction of the lower air gaps ψ_1 and ψ_2. Because of the unbalanced air gap flux density, the motor rotor generates a radial force F_y in the positive y-direction. If the opposite direction current flows into the suspension winding N_2, the radial force along the reverse y-direction can be generated. The radial force along the x-direction can also be obtained by passing a current perpendicular to I_2 through the suspension winding N_2 [33]. The electromagnetic torque that makes the BI motor rotate is the same as the ordinary induction motor, which is based on Lorentz force.

Assuming that the air gap flux density of the motor is B, the Maxwell force acting on the unit area of the outer surface of the rotor can be given by [34].

$$dF_M = \frac{B^2 dA}{2\mu_0} \tag{1}$$

where μ_0 is the vacuum permeability.

The components along the x-axis and y-axis directions are expressed as

$$dF_x(\varphi) = \frac{lr}{2\mu_0} B^2(\varphi)\cos\varphi d\varphi \tag{2}$$

$$dF_y(\varphi) = \frac{lr}{2\mu_0} B^2(\varphi)\sin\varphi d\varphi \tag{3}$$

where l is the effective core length, r is the outer diameter of the rotor and φ is the Spatial location angle.

Since the resultant air gap flux density in the motor is generated by the torque winding and the suspension winding.

$$B(\varphi) = B_2\cos(\varphi + \mu - \omega_1 t) + B_1\cos(2\varphi + \lambda - \omega_1 t) \tag{4}$$

By substituting (4) into (2) and (3), and integrating it, the components of Maxwell force in the x-axis and y-axis directions are obtained as [35].

$$F_x = \frac{lr\pi B_2 B_1}{2\mu_0}\cos(\lambda - \mu) \tag{5}$$

$$F_y = -\frac{lr\pi B_2 B_1}{2\mu_0}\sin(\lambda - \mu) \tag{6}$$

where λ and μ are the initial phase angles, respectively. The subscript 2 and 1 correspond to the torque winding and the suspension winding,

respectively, and the following are the same. Because the suspension windings mainly play the role of suspension, $\psi_{1m} = L_{1m}i_{s1}$ can be considered approximately. Then the coordinate transformation of the formula (4) is carried out, and the Maxwell force in the synchronous rotating coordinate system can be obtained.

$$F_d = K_M(i_{s1d}\psi_{2md} + i_{s1q}\psi_{2mq}) \tag{7}$$

$$F_q = K_M(i_{s1q}\psi_{2md} - i_{s1d}\psi_{2mq}) \tag{8}$$

Among them,

$$K_M = \frac{\pi p_2 p_1 L_{m1}}{12lr\mu_0 W_2 W_1}$$

where W_2 and W_1 the number of coils corresponding to windings, respectively, ψ_{2md} and ψ_{2mq} are the straight and cross axis components of the air-gap flux linkage of the torque winding, respectively, i_{s1d} and i_{s1q} are the straight and cross axis components of the suspension winding current, respectively, L_{m1} is the mutual inductance of the suspension winding. Air gap magnetic field oriented control can be as follows.

$$\psi_{2md} = \psi_{2m} \tag{9}$$

$$\psi_{2mq} = 0 \tag{10}$$

Then the radial suspension force of the rotor is expressed as

$$F_d = K_M i_{s1d}\psi_{2m} \tag{11}$$

$$F_q = K_M i_{s1q}\psi_{2m} \tag{12}$$

It can be concluded that when the flux linkage of the torque winding remains unchanged, the radial suspension force can be adjusted by controlling the components of the *d*-axis and the *q*-axis of the suspended winding current.

Finite element analysis

To study the influence of the magnetic wedge on the performance of the BI motor, a 3-kW, 380 V BI motor is used. The specifications and major dimensions of the three-phase BI motor are shown in Table 1. The magnetic wedges in the BI motor structure are usually supported by wood or insulating material to make the coils fixed in the slot [36]. In this paper, the performance of BI motors is researched by the finite element (FEA) method.

Fig. 2 shows the model of the BI motor stator slot with a magnetic wedge, where the wedge-shaped design is conducted to homogenate the gap discontinuities in the existence of the slot and make the structure easier. In practice, In order to obtain each workpiece of the motor, magnetic material made of magnetic wedge can be used in different plates. Magnetic wedges are the same as those used in the construction of medium voltage motors. The wedges are made of glass fibers, in which epoxy resin and ferrous powder are treated as adhesives. It is extensively applied and tested in practical situations.

Because of the high resistivity of the magnetic wedge material, the influence of the eddy current loss can be ignored. In addition, as the temperature increases, the resistivity will gradually increase, so the effect of the eddy current loss is not obvious. It is concluded that the magnetic loss on the wedge can be ignored.

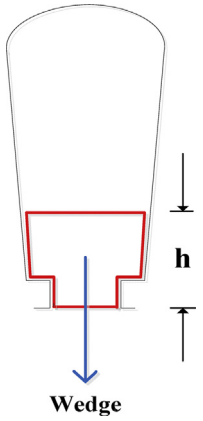

Fig. 2. Semi-closed slot and wedge.

In order to consider the effects of magnetic loss, the magnetic loss characteristics and motor material data provided by the manufacturer have been considered in the simulation model. In the establishment of the motor model, the temperature affecting the magnetic loss is neglected, but the material characteristic loss corresponds to the motor material under working conditions is under consideration. However, recent research has shown that hysteresis and eddy current losses will almost not reduce within the normal working temperature of industrial motors [37]. All other parameters used in the model, such as copper resistivity, are obtained on the prototype under the test temperature.

Table 2 shows the effect of changing the relative permeability on the BI motor when the height of the magnetic wedge is fixed. For this special situation, the height of the wedge is set to 3 mm, and the relative permeability changes between 1 and 10. With respect to losses, it can be observed that with the increase of magnetic permeability, the loss of the stator copper shows a higher decrease. On the contrary, the iron loss is slightly reduced. The efficiency of the motor eventually increased to $\mu_r = 8$, and then began to decline. This phenomenon can be interpreted by a fact that the copper loss of the stator will no longer decrease in excess of a certain μ_r value. The small change in the stray loss actually leads to the deterioration of the motor performance.

Table 3 shows the effect of the variation of the magnetic wedge height on the BI motor when the relative permeability is fixed. From Table 3, it shows that, like the relative permeability, the performance of the BI motor is slightly changed as the wedge height increases, but the performance of the motor with the wedge height exceeding a certain height will begin to decrease. Therefore, the results show that the wedge height has less effect on the performance of the BI motor compared with the relative permeability.

Fig. 3 illustrates the impact on the efficiency of the motor as the wedge height and relative permeability are constantly changing. Higher wedges can achieve better motor performance. It can be observed that the optimum relative permeability value can be found, and when the optimum permeability value is exceeded, the motor efficiency starts to decrease. It can be concluded that the best results are obtained for a 3 mm high wedge with $\mu_r = 8$. In this special case, the efficiency of the

Table 1
Motor specifications and major dimensions.

Items	Values
Rated power	3 kW
Rated voltage	380 V
Rated frequency	50 Hz
Stator slots number	48
Rotor slots number	44
Pole pairs of torque windings	2
Pole pairs of suspension windings	1

Table 2
Comparison table of simulation results.

Performance (h = 2.5 mm)	$\mu_r = 1$	$\mu_r = 3$	$\mu_r = 5$	$\mu_r = 8$	$\mu_r = 10$
Power factor	0.77	0.77	0.78	0.78	0.78
Stator copper loss (W)	152	141	138	138	138
Rotor copper loss (W)	80	76	75	77	78
Iron loss (W)	85	78	74	74	74
Stray loss (W)	42	37	21	20	23
Efficiency (%)	83.21	84.49	85.03	84.82	84.78

Table 3
Comparison table of simulation results.

Performance (μ_r = 5)	h = 2	h = 2.5	h = 3
Power factor	0.76	0.76	0.75
Stator copper loss (W)	138	138	139
Rotor copper loss (W)	74.5	75	72.5
Iron loss (W)	75	74	74
Stray loss (W)	23	21	25
Efficiency (%)	84.93	85.03	84.91

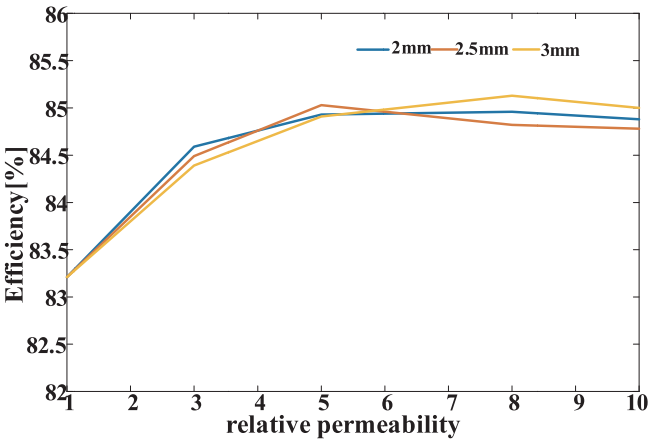

Fig. 3. Efficiency under different magnetic wedge variables.

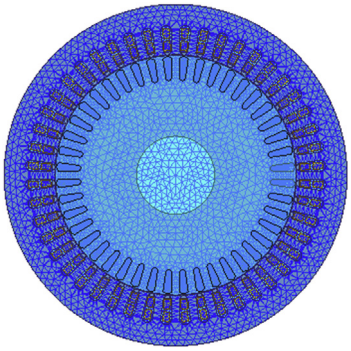

Fig. 4. Mesh view of motor.

motor is better than that of the original. Fig. 4 shows the mesh generation in the model.

Fig. 5 shows flux line distribution when using magnetic wedge and

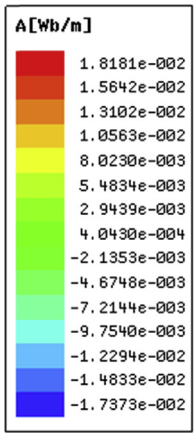

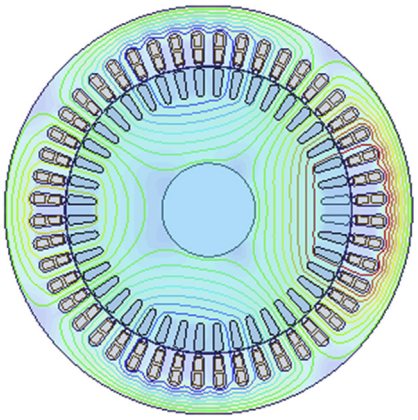

Fig. 5. Flux line plot.

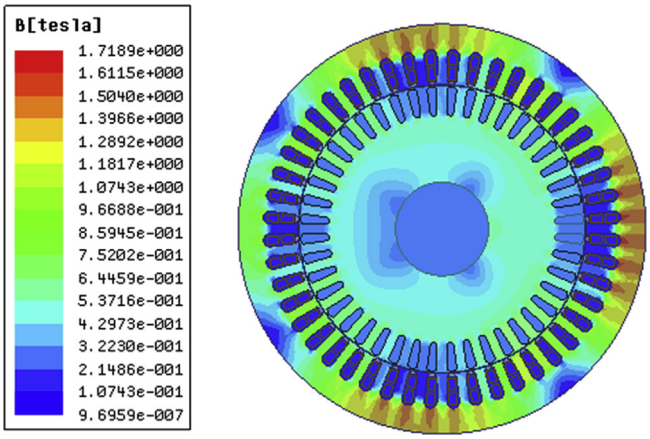

Fig. 6. Magnetic flux density plot.

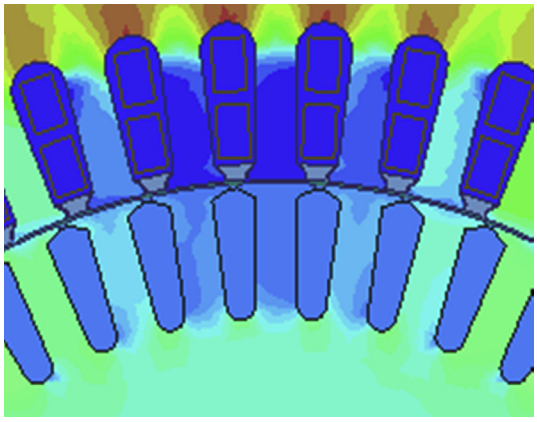

Fig. 7. Magnetic flux density with magnetic wedge μ_r = 8.

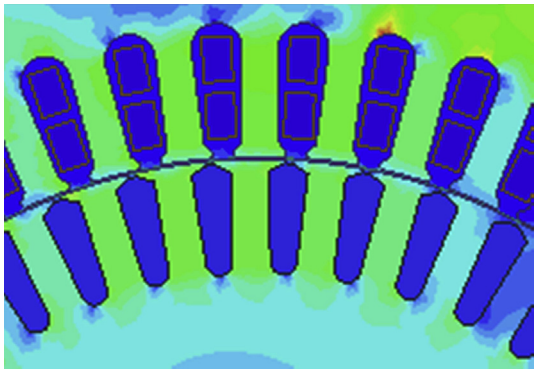

Fig. 8. Magnetic flux density without magnetic wedges.

Fig. 6 shows magnetic flux density when using magnetic wedge. It can be observed that the use of the magnetic wedge has no effect on the flux line distribution and the magnetic flux density. Figs. 7 and 8 show the comparison of the variation in the flux density distribution in the model. It can be seen that the magnetic flux density of magnetic wedge in the stator slots is significantly different from that without magnetic wedge.

Figs. 9 and 10 show the comparison of the output torque with and without magnetic wedges under no-load conditions. The FEA results show that the starting torque using magnetic wedges is reduced compared to the torque without wedges. When using higher relative permeability, the magnetic wedge will greatly reduce the output torque by about a small half of the no-load torque. Therefore, after using the magnetic wedge, the efficiency of the BI motor can be effectively

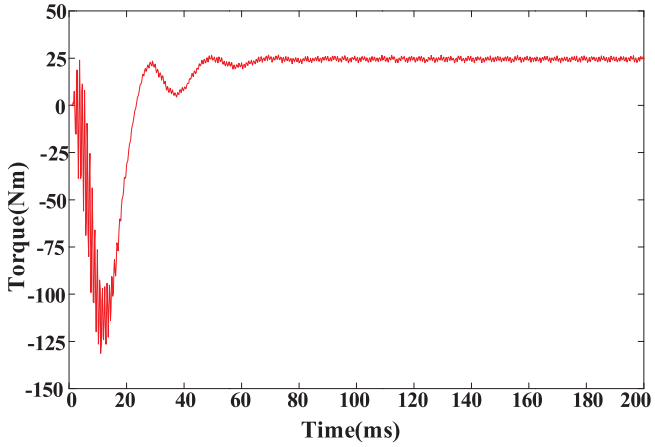

Fig. 9. Torque output using magnetic wedge $\mu_r = 8$.

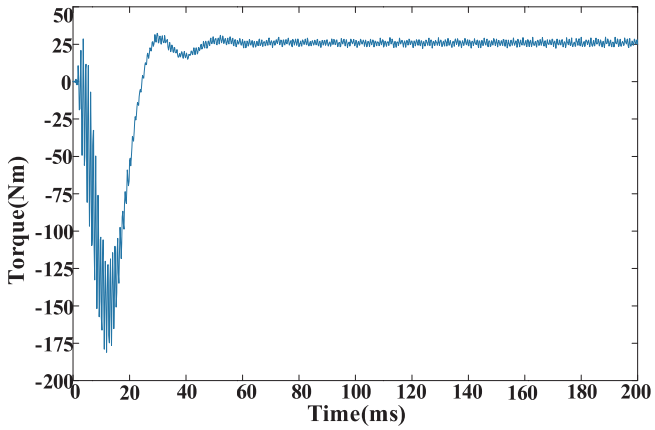

Fig. 10. Torque output without magnetic wedges.

improved. Moreover, it can be concluded that a higher efficiency value can be achieved by reducing the starting torque.

The air flux density using magnetic wedges of relative permeability $\mu_r = 8$ and no wedges is shown in Figs. 11 and 12. This figure shows that when magnetic wedges are used, the ripple of the magnetic flux density in the air gap is relatively reduced. This ability to reduce air gap flux ripple will help reduce pulsation losses. The larger the width of the motor slot, the smaller the average air gap length and the greater the surface loss. The pulse amplitude of the air gap flux density using the magnetic wedge is significantly reduced, so the motor surface loss is reduced. However, as can be seen from the figure, the amplitude of the first half of the air gap flux is slightly decreased, and the amplitude of

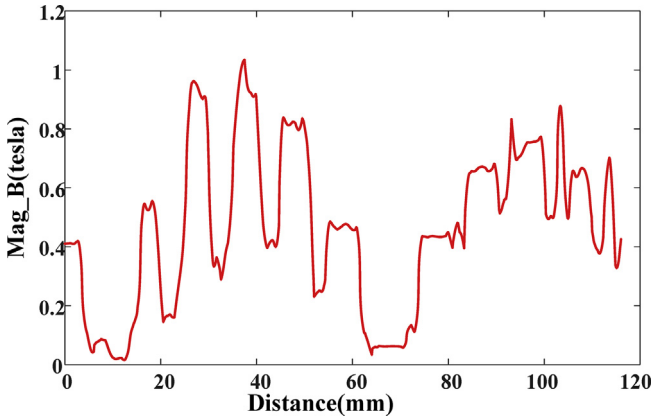

Fig. 11. Air flux density using magnetic wedge $\mu_r = 8$.

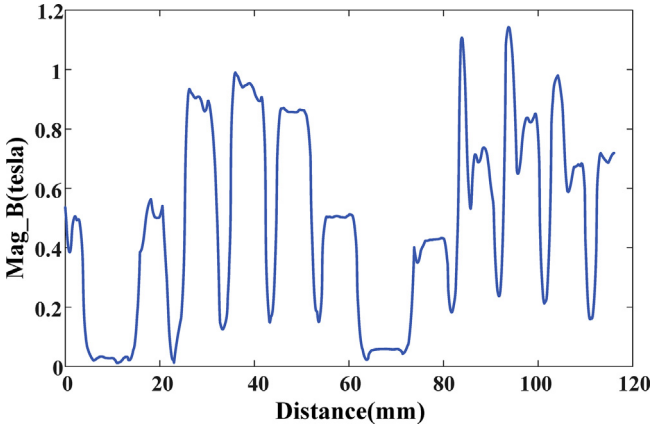

Fig. 12. Air flux density without magnetic wedges.

the latter half is greatly decreased. The magnetic flux can flow through part of the wedge, and the distribution of the air gap flux density tends to be uniform, so noise and vibration can be reduced. This is very beneficial to improve the performance of the BI motor.

Figs. 13 and 14 show the comparison of core loss with and without magnetic wedges under the same conditions. The test results show that the core loss using magnetic wedges decrease as compared to the core loss without wedges. From the above figure, we can observe that as the magnetic permeability increases, the core loss shows a higher reduction. So the performance of the BI motor has been improved. Fig. 15 shows a comparison of three-phase flux linkage with and without magnetic wedges. Before 40 ms, the magnitude of the three phase flux linkage with magnetic wedge is slightly larger than that without magnetic wedge. After 40 ms, the three phase flux linkage with the magnetic wedge coincides with that without the magnetic wedge. It can be concluded that a BI motor using a magnetic wedge has no effect on the three-phase flux linkage.

Fig. 16 illustrates the comparison of the radial suspension force components when the BI motor rotor is eccentric along the *Y*-axis. Fig. 17 illustrates the comparison of the resultant suspension force *F*(N) obtained by changing the eccentricity in the *Y*-axis direction. Whenever the current enters the torque winding and suspension winding with $\theta = 0^\circ$ at the concentric position of the rotor, the resultant suspension force is substantially directed to the right side of the *X*-axis. When the rotor is eccentrically displaced, the one-sided magnetic pull will be generated. From Fig. 16, when the rotor of the BI motor moves in the *Y*-axis direction, the change in the suspension force is significant because the length of the air gap in the *Y*-axis direction varies greatly. Moreover, with the increase of the rotor eccentricity along the *Y*-axis, the amplitude of F_y is symmetric on the whole. It can be observed that the

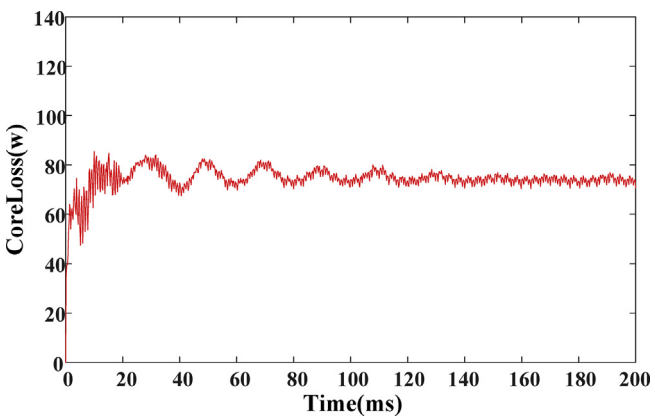

Fig. 13. Core Loss with magnetic wedge $\mu_r = 8$.

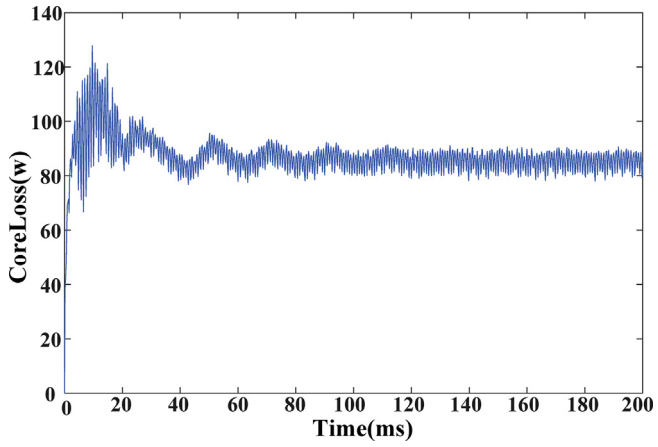

Fig. 14. Core Loss without magnetic wedges.

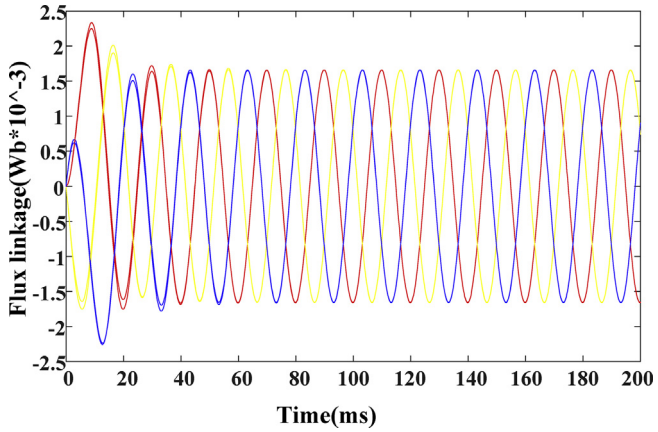

Fig. 15. Three-phase flux linkage comparison.

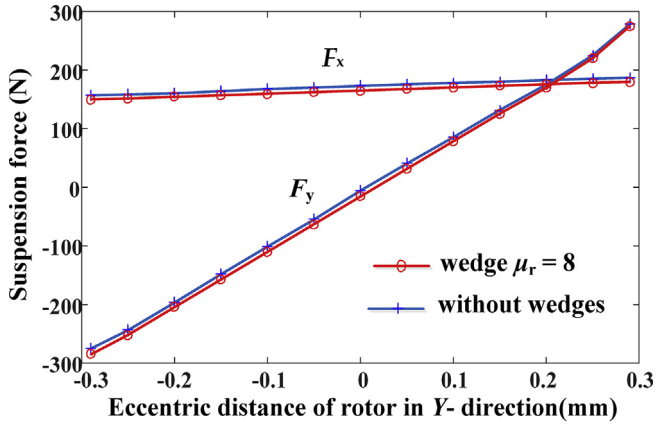

Fig. 16. Suspension force components comparison.

radial suspension force F_y is almost proportional to the eccentric distance of the rotor. However, since the motor air gap length in the *X*-axis direction is substantially constant, the value of F_x will only change within a certain range. In addition, the value of F_x when the rotor eccentric distance is positive is slightly larger than that when the eccentric distance is negative. Therefore, as shown in Fig. 17, the resultant suspension force *F*(N) is not symmetrical.

Fig. 18 illustrates the comparison of the radial suspension force components when the BI motor rotor is eccentric along the *X*-axis. Fig. 19 illustrates the comparison of the resultant suspension force *F*(N) obtained by changing the eccentricity in the *X*-axis direction. As shown

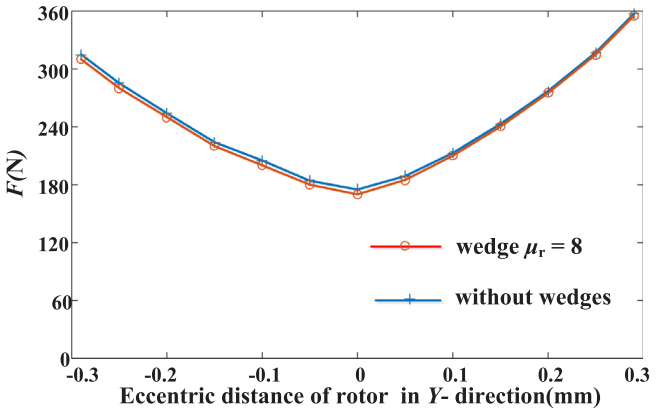

Fig. 17. The resultant suspension force comparison.

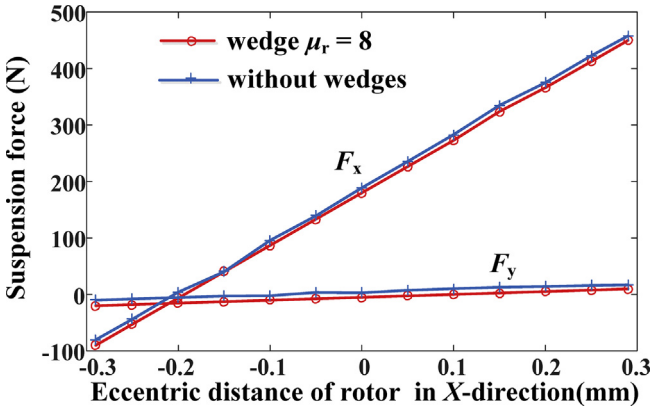

Fig. 18. Suspension force components comparison.

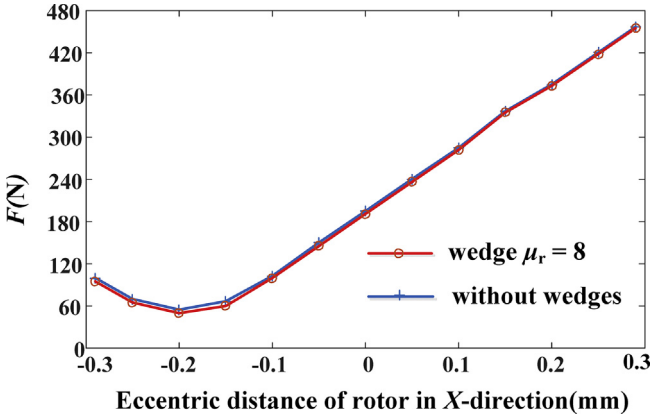

Fig. 19. The resultant suspension force comparison.

in Fig. 18, when the motor rotor is eccentrically left and right in the *X*-axis direction, the change in the radial suspension force is remarkable. In addition, when the eccentric distance of the motor rotor on the *X*-axis is positive, the suspension force generated by the current flowing into the suspension winding acts on the magnetic pull on one side. Therefore, the amplitude of F_x is almost proportional to the eccentricity of the motor rotor. When the eccentric distance of the motor rotor on the *X*-axis is negative, the one-sided magnetic pull force can cancel the generated suspension force. Therefore, as the negative eccentricity of the motor rotor on the *X*-axis increases, the F_x amplitude is slowly decreased first, but in the case where the one-sided magnetic pulling force is increased, it is slowly increased in the opposite direction gradually. The results are shown in Fig. 19. The change of the resultant suspension force *F*(N) is gradually decreasing and then increasing significantly.

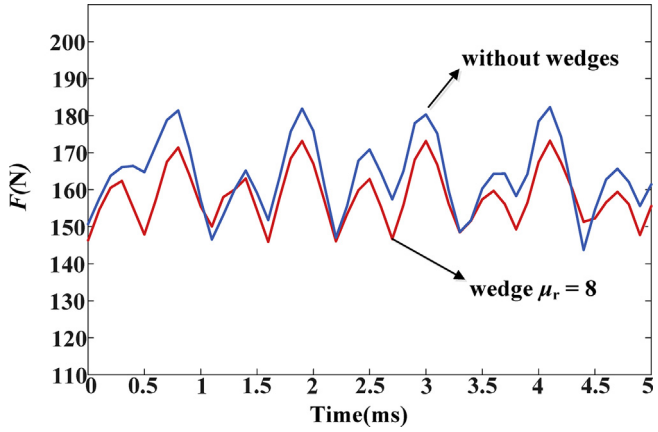

Fig. 20. The resultant suspension force F(N) comparison.

From Figs. 17 to 19, it can be observed that adding a magnetic wedge in the BI motor has little effect on the suspension force. From Fig. 20, the suspension force has smaller fluctuations and the stability becomes stronger. Therefore, it is of great significance to add magnetic wedge into stator slot in BI motors.

Discussion

In recent years, the big challenge for manufacturers is to improve the performance of all aspects of the motor [38]. The current analysis shows that the use of magnetic wedge in the BI motor stator slot is a very effective measure, which can significantly improve the performance of motor. After the above comparison results, the torque fluctuation, efficiency and suspension force of the BI motor are improved. When using a magnetic wedge, the load current and starting torque decrease, which will improve the efficiency of the motor. However, the performance torque decreases slightly over the entire speed range. Another interesting place for this proposal is its economic aspect [39]. Although it is not clear that the cost per unit increases when using magnetic wedge, so far, it is lower than the cost of other alternatives.

The FEA shows that the output performance of the BI motor drops sharply when the permeability value set in the magnetic wedge becomes too large. Speaking generally, the optimum permeability value is highly optimized for the BI motor. In addition, the result proves that the finite element analysis is very effective to determine the optimal wedge specification.

Conclusion

In this paper, a research method that can improve the performance of BI motor is analyzed. This strategy reduces the air gap reluctance, which decreases the stator current and the core loss. Therefore, the performance of BI motor has been enhanced in many ways. At present, effective improvement of the performance of the motor is urgently needed in the industry. The proposed solution is to reduce the loss of BI motor and increase its stability. Installing a suitable magnetic wedge in a BI motor is an effective measure to improve its performance, and it is still an interesting research subject in the field of motors.

Acknowledgments

This work was supported by the National Natural Science Foundation of China under Projects 51875261 and 51475214, the Natural Science Foundation of Jiangsu Province of China under Projects BK20180046 and BK20170071, the Six Categories Talent Peak of Jiangsu Province under Projects 2016-GDZB-096 and 2015-XNYQC-003, the “Qinglan project” of Jiangsu Province, the Key Project of Natural Science Foundation of Jiangsu Higher Education Institutions under Project 17KJA460005, the “333 project” of Jiangsu Province under Project BRA2017441, and the Priority Academic Program Development of Jiangsu Higher Education Institutions (PAPD).

References:

[1] Gerada D, Mebarki A, Brown NL, Gerada C. High-speed electrical machines: technologies, trends, and developments. IEEE Trans Ind Electron 2014;61(6):2946–59.
[2] Sun X, Chen L, Yang Z. Overview of bearingless permanent magnet synchronous motors. IEEE Trans Ind Electron 2013;60(12):5528–38.
[3] Abdel-Khalik AS, Ahmed S, Massoud A. A bearingless coaxial magnetic gearbox. Alexandria Eng J 2014;53(3):573–82.
[4] Zhang W, Zhu H. Radial magnetic bearings: an overview. Results Phys 2017;7:3756–66.
[5] Zhu X, Xiang Z, Quan L, Wu W, Du Y. Multi-Mode optimization design methodology for a flux-controllable stator permanent magnet memory motor considering driving cycles. IEEE Trans Ind Electron 2018;65(7):5353–66.
[6] Çıra F. Detection of eccentricity fault based on vibration in the PMSM. Results Phys 2018;10:760–5.
[7] Sun X, Su B, Wang S, Lei ZG, Zhu J, Guo Y. Performance analysis of suspension force and torque in an IBPMSM with V-shape PMs for flywheel batteries. IEEE Trans Magn 2018;54(11):2827103. https://doi.org/10.1109/TMAG.
[8] Cao X, Deng Z. A full-period generating mode for bearingless switched reluctance generators. IEEE Trans. Appl. Supercond 2010;20(3):1072–6.
[9] Chiba A, Asama J. Influence of rotor skew in induction type bearingless motor. IEEE Trans. Magn 2012;48(11):4646–9.
[10] Duan N, Xu W, Wang S, Zhu J. Current distribution calculation of superconducting layer in HTS cable considering magnetic hysteresis by using XFEM. IEEE Trans Magn 2018;54(3):8000804.
[11] Sun X, Shi Z, Chen L, Yang Z. Internal model control for a bearingless permanent magnet synchronous motor based on inverse system method. IEEE Trans Energy Convers 2016;31(4):1539–48.
[12] Duan N, Xu W, Wang S, Zhu J. Accuracy analysis of structure with nearby interfaces within XFEM. AIP Adv 2017;7(5):056011.
[13] Lei G, Liu CC, Zhu JG, Guo YG. Techniques for multilevel design optimization of permanent magnet motors. IEEE Trans Energy Convers 2015;30(4):1574–84.
[14] Asama J, Oi T, Oiwa T, Chiba A. Simple driving method for a 2-DOF controlled bearingless motor using one three-phase inverter. IEEE Trans Ind Appl 2018;54(5):4365–76.
[15] Lei G, Wang TS, Zhu JG, Guo YG, Wang SH. System level design optimization method for electrical drive systems: deterministic approach. IEEE Trans Ind Electron 2014;61(12):6591–602.
[16] Minaz MR, Çelebi M. Design and analysis of a new axial flux coreless PMSG with three rotors and double stators. Results Phys 2017;7:183–8.
[17] Sun X, Chen L, Yang Z, Zhu H. Speed-sensorless vector control of a bearingless induction motor with artificial neural network inverse speed observer. IEEE/ASME Trans Mechatron 2013;18(4):1357–66.
[18] Curiac R, Li H. Improvements in energy efficiency of induction motors by the use of magnetic wedges. IEEE IAS Annu Meeting PCIC 2011;1–6.
[19] Skalka M, Ondrusek C, Kurfurst J, Cipin R. Harmonic reduction in induction machine using slot wedges optimization. International Symposium on Power Electronics, Electrical Drives, Automation and Motion (SPEEDAM) 2012:1252–5.
[20] Mikami H, Ide K, Takahashi M, Kajiwara K. Dynamic harmonic field analysis of a cage type induction motor when magnetic slot wedges are applied. IEEE Trans. Energy Convers 1997;12:337–43.
[21] Sun X, Chen L, Jiang H, Yang Z, Chen J, Zhang W. High-performance control for a bearingless permanent magnet synchronous motor using neural network inverse scheme plus internal model controllers. IEEE Trans Ind Electron 2016;63(6):3479–88.
[22] Kappatou J, Gyftakis C, Safacas A. A study of the effects of the stator slots wedges material on the behavior of an induction machine. Proceedings of the 2008 international conferences on electrical machines. 2008. paper ID 949.
[23] de Almeida AT, Ferreira FJTE, Ge B. Beyond induction motors—technology trends to move up efficiency. IEEE Trans Ind Appl 2014;50(3):2103–41.
[24] Kaga A, Anazawa Y, Akagami H. The efficiency of capacitor motor with ferrite magnetic wedges. IEEE Trans Magn 1986;25(5):964–6.
[25] Takeda Y, Yagisawa T, Suyama A, Yamamoto M. Application of magnetic wedges to large motors. IEEE Trans Magn 1984;20(5):1780–2.
[26] De Almeida A, Ferreira F, Quintino Duarte A. Technical and economical considerations on super high-efficiency three-phase motors. Ind Appl, IEEE Trans 2014;50(2):1274–85.
[27] Sun X, Su B, Chen L, Yang Z, Chen J, Zhang W. Nonlinear flux linkage modeling of a bearingless permanent magnet synchronous motor based on AW-LSSVM regression algorithm. Int J Appl Electromagnet Mech 2016;51(2):151–9.
[28] Dietz D, Messager G, Binder A. 1kW/60,000min^{-1}bearingless PM motor with combined winding for torque and rotor suspension. IET Electr Power Appl 2018;12(8):1090–7.
[29] Sun X, Xue Z, Zhu J, Guo Y, Yang Z, Chen L, et al. Suspension force modeling for a bearingless permanent magnet synchronous motor using Maxwell stress tensor method. IEEE Trans Appl Supercond 2016;26(7):0608705.
[30] Huang J, Li B, Jiang H, et al. Analysis and control of multiphase permanent-magnet bearingless motor with a single set of half-coiled winding. IEEE Trans Ind Electron 2014;61(7):3137–45.
[31] Le Y, Fang J, Wang K. Design and optimization of a radial magnetic bearing for

high-speed motor with flexible rotor. IEEE Trans Magn 2015;51(6):1–13.
[32] Lei G, Wang TS, Zhu JG, Guo YG, Wang SH. System-level design optimization method for electrical drive systems – robust approach. IEEE Trans Ind Electron 2015;62(8):4702–13.
[33] Yaseen MHA, Abd HJ. Modeling and control for a magnetic levitation system based on SIMLAB platform in real time. Results Phys 2018;8:153–9.
[34] Sun X, Su B, Chen L, Yang Z, Xu X, Shi Z. Precise control of a four degree-of-freedom permanent magnet biased active magnetic bearing system in a magnetically suspended direct-driven spindle using neural network inverse scheme. Mech Syst Sig Process 2017;88:36–48.
[35] Liu C, Zhu J, Wang Y, et al. Comparison of electrical machines with SMC core. IEEE Trans Ind Electron 2017;64(2).
[36] Lavanya M, Selvakumar P, Vijayshankar S, Easwarlal C. Performance analysis of three phase induction motor using different slot wedges. IEEE 2nd international conference on electrical systems. 2014. p. 164–7.
[37] Sun X, Shen Y, Wang S, Lei Gang, Yang Z, Han S. Core losses analysis of a novel 16/10 segmented rotor switched reluctance BSG motor for HEVs using nonlinear lumped parameter equivalent circuit model. IEEE/ASME Trans Mechatron 2018;23(2):747–57.
[38] Ma B, Lei G, Zhu JG, Guo YG, Liu CC. Application-oriented robust design optimization method for batch production of permanent-magnet motors. IEEE Trans Ind Electron 2018;65(2):1728–39.
[39] Donolo PD, Bossio GR, De Angelo C. Analysis of voltage unbalance effects on induction motors with open and closed slot. Energy Convers Manag 2011;52(5):2024–30.